Journal of Magnetism and Magnetic Materials 349 (2014) 173–179

Contents lists available at ScienceDirect

Journal of Magnetism and Magnetic Materials

journal homepage: www.elsevier.com/locate/jmmm

Magnetic order and dynamical properties of the spin-frustrated magnet $Dy_{2-x}Yb_xTi_2O_7$

Hui Liu, Youming Zou, Lei Zhang, Langsheng Ling, Hongyan Yu, Lei He, Changjin Zhang *, Yuheng Zhang

High Magnetic Field Laboratory, Chinese Academy of Sciences and University of Science and Technology of China, Hefei 230031, China

ARTICLE INFO

Article history:
Received 8 June 2013
Received in revised form
17 August 2013
Available online 7 September 2013

Keywords:
Pyrochlore
Hybrid frustrated magnet
Spin interaction
Crystalline electric field

ABSTRACT

The magnetic order and dynamical properties of spin-frustrated magnet $Dy_{2-x}Yb_xTi_2O_7$ single crystals have been studied by dc and ac susceptibility measurements. It is found that the substitution of the Dy^{3+} by the Yb^{3+} in $Dy_2Ti_2O_7$ relaxes ferromagnetic coupling. In low Yb^{3+} doping samples, a spin freezing peak at T_f ($T_f < 3$ K) and a single-ion effect peak T_s associated with Dy^{3+} are observed. With increasing Yb^{3+} doping, a new peak marked by T^* associated with Yb^{3+} appears. We suggest that T^* originates from the thermally activated spin fluctuations of Yb^{3+}. It is also found that the relaxation process for T_s becomes both thermally activated and quantum tunneled in $x \geq 1.0$ samples. The low-temperature dynamical behaviors of $Dy_{2-x}Yb_xTi_2O_7$ are dominated by the Dy–Yb spin interactions and the altered crystalline electric field. Moreover, crystal field-phonon coupling may contribute to the spin dynamic properties.

1. Introduction

Geometrically frustrated magnets have been intensely studied over the past two decades due to their rich variety of unconventional ground states [1]. In particular, pyrochlore oxides with chemical formula $A_2B_2(O1)_6(O2)$, where A^{3+} is a rare-earth ion and B^{4+} is a transition-metal ion, have attracted considerable attention. The pyrochlore lattice is a typical example of geometric frustration in three dimensions, where the spins reside on the vertices of corner-sharing tetrahedra. The atom A occupies the 16*d* and B occupies the 16*c* position and the oxygen atoms O1 and O2 occupy the 48*f* and 8*b* sites, respectively [2]. Among the pyrochlore oxide family, $A_2Ti_2O_7$ are found to display diverse low-temperature properties, such as the formation of spin ice [3,4], spin liquid [1], diverse ordered states [5,6], etc.

The pyrochlore oxide $Dy_2Ti_2O_7$ (DTO) is considered to be a model system of spin ice materials, whose magnetic moments obey the same ordering rule as the proton ordering in water ice. That is, the local spin correlations are characterized by the ice rules: two spins point in and two spins point out of every tetrahedron [7]. Because the ground state is highly degenerate, a static disordered state 'spin ice' is formed below 1 K in spite of the structural order of the system. In addition, Dy^{3+} spins are confined along the local [111] directions due to strong crystal field (CF), rendering a well separated spin ground state doublet at about 200 K below the first excited state [8,9]. The Curie–Weiss temperature θ_{CW}, which is indicative of the nearest-neighbor coupling strength, is of ferromagnetic type with a value of about 1 K [10]. The investigation of ac susceptibility indicates that the spin relaxation in DTO compound exhibits an unusual double crossover upon cooling: its characteristic changes from high temperature thermally activated into quantum tunneling at $T_{cross} \sim 13$ K, and then reverts to thermally activated blow $T_{ice} \sim 4$ K due to the development of spin correlations [11,12].

$Yb_2Ti_2O_7$ (YTO) provides an intriguing contrast to the classical spin ices. Hodges et al. [13] used Mössbauer spectroscopy to investigate the crystal field scheme and determined that the ground-state Kramers doublet is separated by 620 K from the first excited state, producing an easy plane anisotropy. The net inter-ionic interaction is ferromagnetic ($\theta_{CW} = 0.75$ K) and it is dominated by exchange because the dipole–dipole interaction is relatively small due to the modest value, i.e., 1.15 μ_B of the Yb^{3+} moment. A transition takes place at about 0.2 K, but the ground state is not a magnetic long-range-order phase. Most experimental evidence suggests that $Yb_2Ti_2O_7$ displays a disordered ground state down to 30 mK [14–20]. It shows slowly fluctuating Yb^{3+} magnetic moments with short range correlations. Therefore, $Yb_2Ti_2O_7$ is considered to be a 'quantum spin ice' material [14,21].

There have been many reports on the derivative species of rare-earth titanates. There are stuffed compounds where additional rare-earth ions are substituted for the Ti ions, and diluted compounds where nonmagnetic ions are used to dilute the magnetic interactions. By contrast, there are few studies on hybrid rare-earth titanates, which consist of different rare-earth ions on the A sites [22–26]. Recently, Orendac et al. investigated the magnetic order in hybrid frustrated magnets $Gd_{2-x}Tb_xTi_2O_7$ and found that the ground state in the compounds cannot be considered as a simple mixture of ground states present in $Gd_2Ti_2O_7$ and $Tb_2Ti_2O_7$ [26]. In this paper, we report

* Corresponding author. Tel.: +86 551 65595655.
E-mail address: zhangcj@hmfl.ac.cn (C. Zhang).

0304-8853/$ - see front matter © 2013 Elsevier B.V. All rights reserved.
http://dx.doi.org/10.1016/j.jmmm.2013.08.062

the magnetic behaviors of spin-frustrated magnet $Dy_{2-x}Yb_xTi_2O_7$, the mixture compounds of the spin ice $Dy_2Ti_2O_7$ and the quantum spin ice $Yb_2Ti_2O_7$. It is found that the substitution of the Dy^{3+} by the Yb^{3+} in $Dy_2Ti_2O_7$ relaxes ferromagnetic coupling. The magnetic dynamical behavior is related to the Dy–Yb spin interactions and the altered crystalline electric field.

2. Experiments

The single-crystal samples were prepared by the traveling solvent floating zone technique. Firstly, polycrystalline samples of $Dy_{2-x}Yb_xTi_2O_7$ $(0 \le x \le 2)$ were prepared by firing stoichiometric amounts of Dy_2O_3, Yb_2O_3 and TiO_2 up to 1400 °C for several days with intermittent grindings to ensure a complete reaction. Large single crystals of $Dy_{2-x}Yb_xTi_2O_7$ (DYTO) were subsequently grown by the traveling solvent floating zone method under oxygen atmosphere. Details of the crystal growth were described elsewhere [27].

The obtained crystals were characterized by powder x-ray diffraction (XRD) and x-ray single-crystal diffraction with Cu Kα radiation at room temperature. The principal axes were determined using the Laue diffraction patterns. The dc susceptibility, magnetization and the ac susceptibility were measured using the Quantum Design SQUID magnetometer. The real and imaginary parts of the ac susceptibility, χ' and χ'', were determined using an excitation field of $H_{ac}=3.5$ Oe at frequencies spanning $f=10$ to 1000 Hz. The dc and ac susceptibility data were corrected for the demagnetization factor. In this article we report the magnetization data for a field applied along the [111] axis, which is an easy-axis direction for the spin-ice system $Dy_2Ti_2O_7$ but a hard-axis direction for ferromagnetic *XY* pyrochlore $Yb_2Ti_2O_7$.

3. Results and discussion

Fig. 1(a) gives the x-ray-diffraction (XRD) patterns of a representative single crystal with the (l l l) reflections (the black curve) and the $Dy_{2-x}Yb_xTi_2O_7$ $(0 \le x \le 2.0)$ powder samples. We notice that the full width at half maximum (FWHM) for all the diffraction peaks shown in the single crystal XRD pattern is less than 0.15°, indicating the high quality of the sample. To examine the purity of the prepared crystals, we perform powder XRD measurements by grinding the single crystals into powder. No impurity peak is found in the XRD patterns. The analysis of the powder XRD patterns confirms that all samples are crystallized in face-centered-cubic pyrochlore structure with space group Fd-3m. The lattice parameters of the DYTO series are displayed in Fig. 1(b). The lattice constant is found to be in proportion to the composition x, obeying Vegard's law. This linear dependence and the fact that no peak splitting was observed in XRD patterns indicate that a complete mixing of the cations can be achieved and no phase separation occurs in the DYTO samples.

Fig. 2(a) shows the temperature dependence of magnetization for the samples measured along the [111] direction. The magnetic field is 100 Oe. Since there is no difference between zero-field-cooling (ZFC) process and field-cooling (FC) process, we plot only the FC curves. All the samples closely follow the canonical paramagnetic behavior, suggesting no magnetic ordering or spin-glass-like transition occurs down to 2 K. The inverse dc susceptibility χ^{-1} for each sample is shown in the inset of Fig. 2(a). The deviation from the linear Curie–Weiss (CW) behavior at low temperature is probably due to some magnetic correlations. At high temperatures (100–300 K), the inverse susceptibility data are

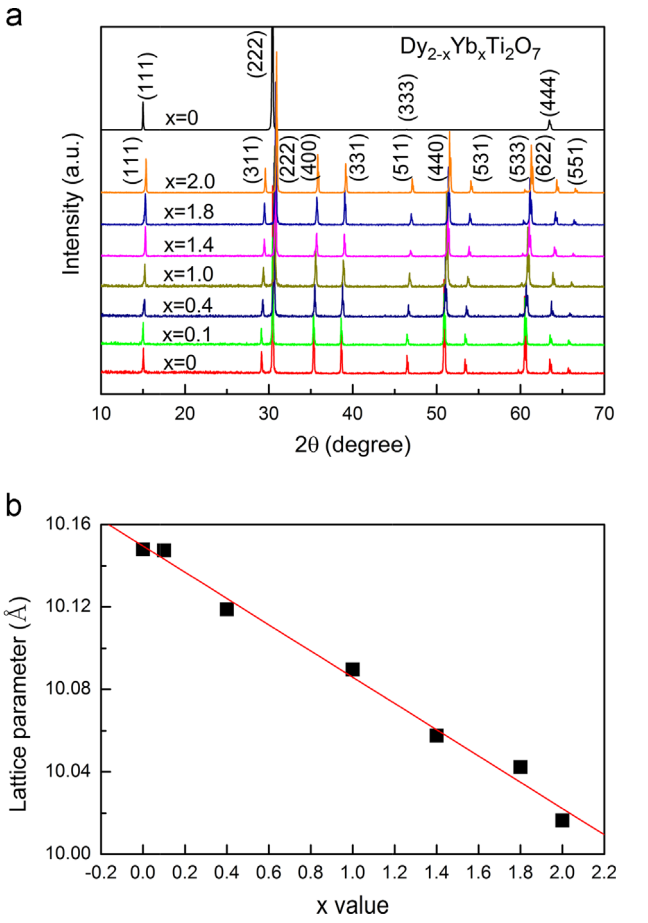

Fig. 1. (a) Powder x-ray-diffraction patterns for the $Dy_{2-x}Yb_xTi_2O_7$ samples. The black curve is the single-crystal XRD pattern of a $Dy_2Ti_2O_7$ sample; (b) The lattice constants of the Yb-doped samples.

fitted using the CW law [10].

$$\chi = \frac{N_A \mu_{eff}^2}{3k_B(T-\theta_{CW})} \quad (1)$$

Where N_A is the Avogadro number, θ_{CW} is the Curie–Weiss temperature, μ_{eff} is the effective magnetic moment, and k_B is the Boltzmann constant. The corresponding θ_{CW} and μ_{eff}/Dy(Yb) for all samples are displayed in Fig. 2(b) and (c), respectively. Unlike the parent material $Dy_2Ti_2O_7$, which has a positive CW temperature, all $Dy_{2-x}Yb_xTi_2O_7$ mixtures show a large negative CW temperature. The negative CW temperatures are due to a high-energy crystal-field level [25], i.e., the thermal population of the excited CF states. Since there are two types of magnetic ions distributed randomly over site A of the pyrochlore $A_2B_2O_7$ structure, one can express the effective magnetic moment μ_{eff} per f.u. as

$$\mu_{eff}^2 = x\mu_{Yb}^2 + y\mu_{Dy}^2 \quad (2)$$

Where x and y are the number of Yb and Dy atoms per f.u., respectively; μ_{Yb} and μ_{Dy} are the effective magnetic moment of Yb and Dy ions, respectively. For the free Dy^{3+} and Yb^{3+} ions, $\mu_{Dy}=10.6\mu_B$/Dy and $\mu_{Yb}=4.5\mu_B$/Yb. The calculated effective moments per Dy(Yb) are also shown in Fig. 2(c) by triangle symbols. The effective moments calculated by CW law and the related ratios of the free moments are close to each other. In fact, results from CW fits are very sensitive to the temperature range used. The CW law also describes the data well between 2–20 K. These data are collected well below the temperature appropriate for the lowest crystal-field excitation and the CW-like temperatures are significantly more ferromagnetic than those collected at

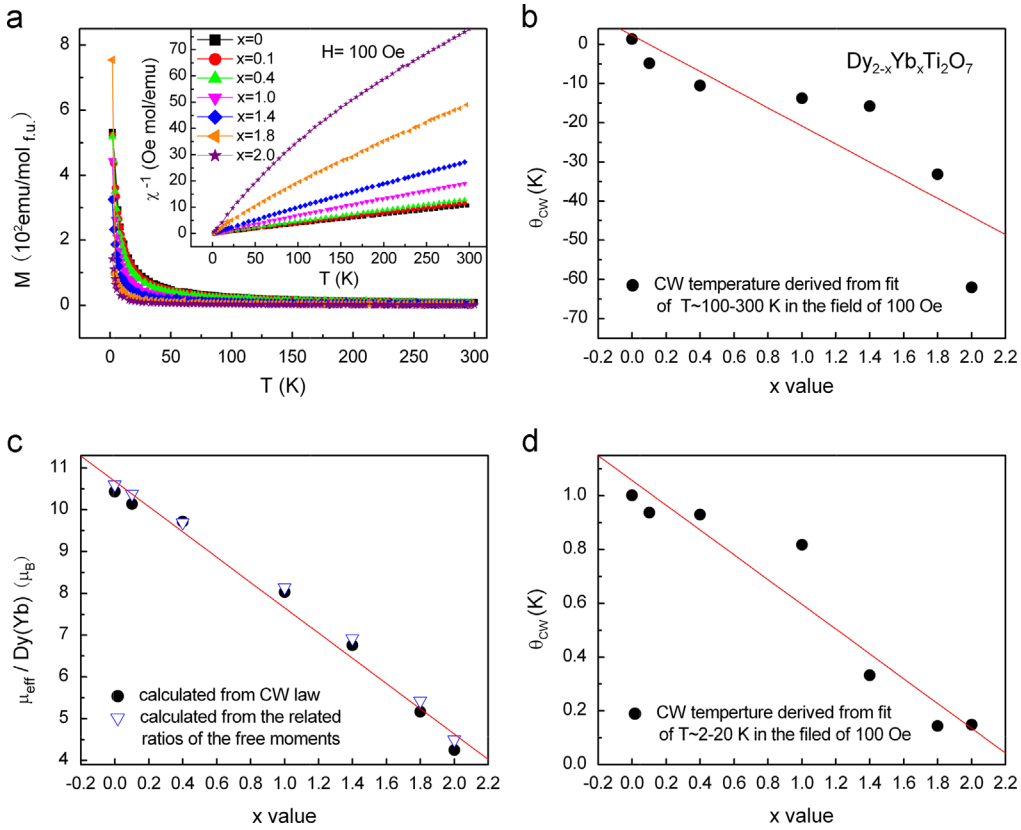

Fig. 2. (a) The temperature dependence of dc magnetic susceptibility of the $Dy_{2-x}Yb_xTi_2O_7$ samples from 2 K to 300 K. In the inset, the corresponding inverse magnetic susceptibility is given; (b) Curie–Weiss (CW) temperatures; and (c) the effective paramagnetic moments derived from CW law at high temperature (100–300 K) ranges for $Dy_{2-x}Yb_xTi_2O_7$; (d) CW temperatures derived from the data between 2–20 K. The lines are a guide to the eye.

higher temperatures (see Fig. 2(d)). We also find that the calculated effective moments at the range of 2–20 K are smaller than those of high temperatures (data not shown). The dependency of θ_{CW} and μ_{eff} on the fitting temperature range is probably related to the large CF splitting of the multiplets Dy^{3+} and Yb^{3+}, which is not taken into account in the fitting procedure. The CW temperature of DTO is qualitatively similar to that of previous report [10] and the CW temperature of YTO is in agreement with that of singe crystal YTO [14]. The susceptibility measurements show a tendency for the effective moment and the CW temperature to decrease with increasing doping, indicative of decreased FM coupling.

The *M–H* curves collected at 2 K for the $Dy_{2-x}Yb_xTi_2O_7$ samples are presented in Fig. 3. The magnetization decreases with increasing Yb concentration. This trend is consistent with the fact that Yb^{3+} has smaller moment compared with that of Dy^{3+}. It should be noticed that with increasing Yb content, the unsaturation behavior in the *M–H* curves becomes more obvious, as shown by the decrease in the slope of *M–H* curves at low fields. This means that $Dy_{2-x}Yb_xTi_2O_7$ mixed compounds have a tendency towards a weaker FM interaction on increasing the Yb concentration, which is consistent with the result derived from *M–T* curves.

In order to get the dynamical properties of the compounds, we measured the ac susceptibility. Figs. 4–6 give the real (χ') and imaginary (χ'') parts of the ac susceptibility of samples for $x=0$, 1.8, and 2.0 respectively with $H=0$, 5 and 10 kOe. For $Dy_2Ti_2O_7$ ($x=0$), as the field increases to 10 kOe, two clear dips in χ' appear near 16 K and 3 K, leading to the corresponding peaks in χ'' as expected from the Kramers–Kronig relations [11,28]. On the basis of the convention of previous reports, the high-temperature peak is assigned to be the single-ion peak of Dy^{3+} spins, which is considered as a freezing of the thermally activated spin flip process via the lowest lying crystal field excitations [29]. However, the low temperature

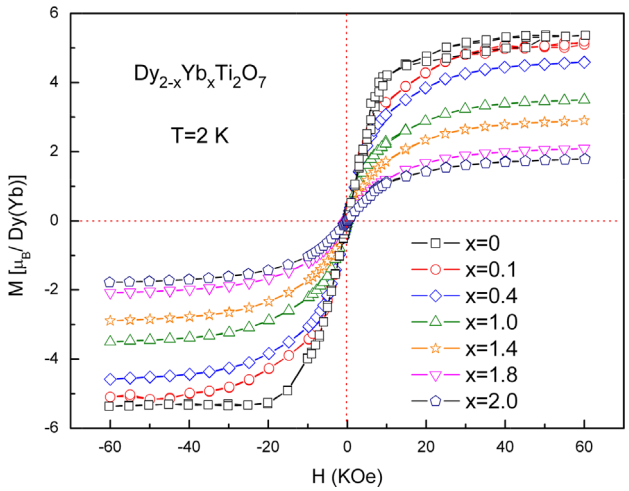

Fig. 3. The magnetic field dependence of the magnetization *M* at T=2 K for a series of $Dy_{2-x}Yb_xTi_2O_7$ compounds.

peak originates from the spin freezing associated with the spin-ice rules [30]. As for $x=1.8$ sample, there are also two peaks in χ'' with high external field. But in the case of $Yb_2Ti_2O_7$ ($x=2$), there is only one peak at low temperatures with the field $H=10$ kOe. We find that for all the samples, χ' represents a canonical paramagnetic behavior at $H=0$. The effect of an externally applied magnetic field is that it slows down the dynamical process in samples and enhances the dips in χ' or the peaks in χ''. Therefore, for the other samples, we measured the ac susceptibility with the high external field $H=10$ kOe.

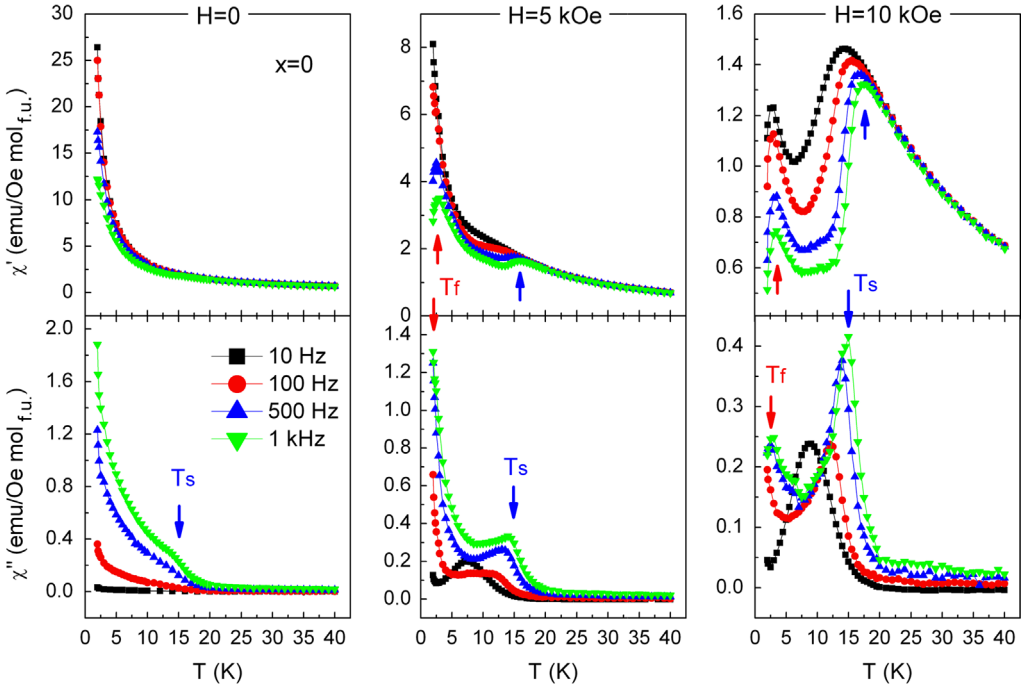

Fig. 4. The real (χ') and imaginary part (χ'') of ac susceptibility of $Dy_2Ti_2O_7$ measured at $H=0$, 5 kOe and 10 kOe. The T_f and T_s are discussed in Fig. 7 and corresponding text.

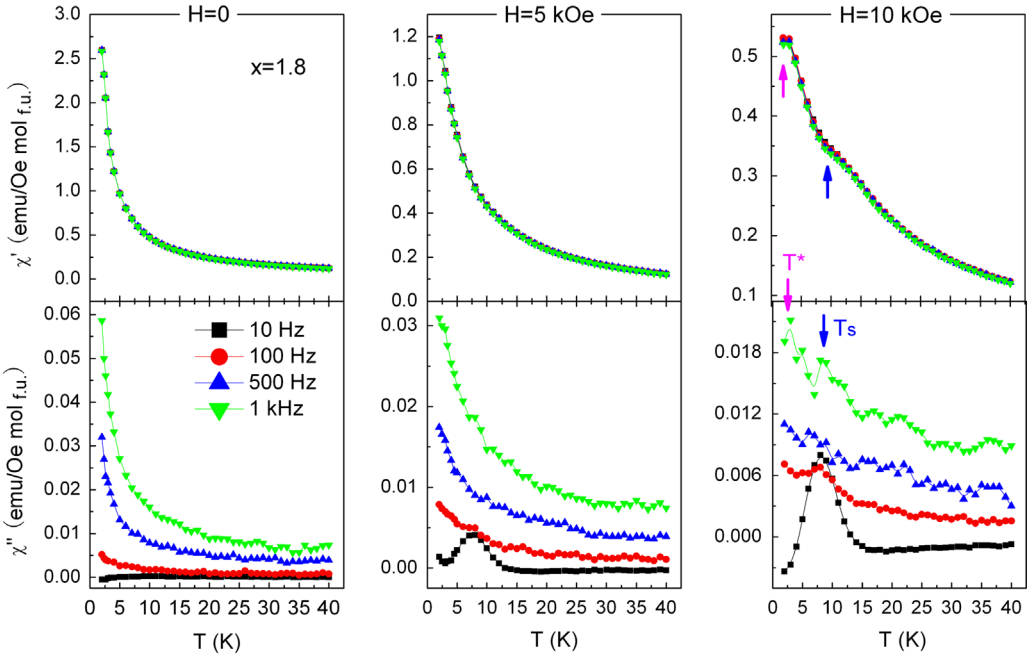

Fig. 5. The real (χ') and imaginary part (χ'') of ac susceptibility of $Dy_{0.2}Yb_{1.8}Ti_2O_7$ measured at $H=0$, 5 kOe and 10 kOe. The T^* and T_s are discussed in Fig. 7 and corresponding text.

Fig. 7 shows the ac susceptibility of samples with $x=0.1$, 0.4, 1.0, 1.4, and 1.8. The applied dc magnetic field is $H=10$ kOe. For the light doping of $x=0.1$, a clear dip appears in χ' around 16 K, and the χ'' shows a peak corresponding to the drop in χ'. At low temperature, another peak in χ'' emerges (marked by T_f). This peak gradually weakens and disappears with increasing Yb doping. At the same time, the high temperature peak (marked by T_s) becomes broader and unobvious until it disappears when $x=2.0$. By analogy to DTO, we therefore identify the high-temperature peak T_s as the single-ion peak of Dy^{3+} spins and the low temperature peak T_f originates from the spin-ice freezing. With increasing Yb doping, an additional peak, indicated by T^*, emerges in $x \geq 1.0$ samples. This peak becomes more pronounced in $x=1.4$, 1.8 and 2.0 samples. The emergence of the peak T^* in $Dy_2Yb_{2-x}Ti_2O_7$ is similar to the case of $Dy_xTb_{2-x}Ti_2O_7$ [24]. The peak T^* should originate from the Yb spins.

The emergence of T_f indicates that the low-doping samples still obey the ice rules, suggesting that spin-ice state is robust against magnetic-moment dilution. In DTO, the long-range dipole–dipole correlation makes the system insensitive to defects. However, the T_f peak disappears in heavily doped samples, indicating that the spin-ice rules are broken. For pure DTO, the nearest-neighbor exchange interaction is $J_{nn}=-1.24$ K and the nearest dipolar interaction is $D_{nn}=2.35$ K [7]. While for pure YTO, the dipolar

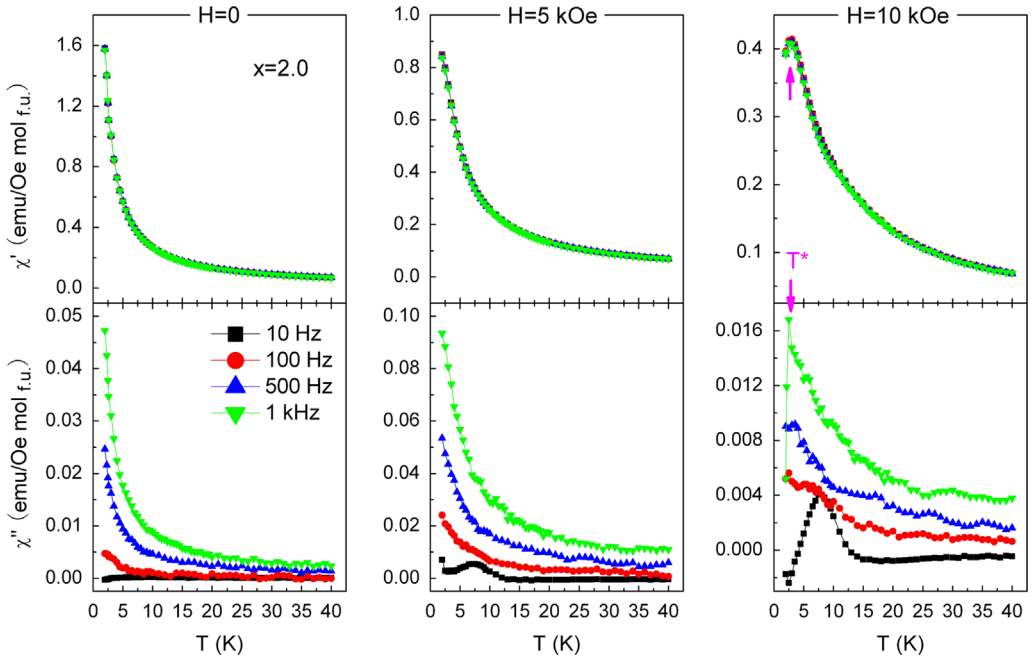

Fig. 6. The real (χ') and imaginary part (χ'') of ac susceptibility of $Yb_2Ti_2O_7$ measured at $H=0$, 5 kOe and 10 kOe. The T^* is discussed in Fig. 7 and corresponding text.

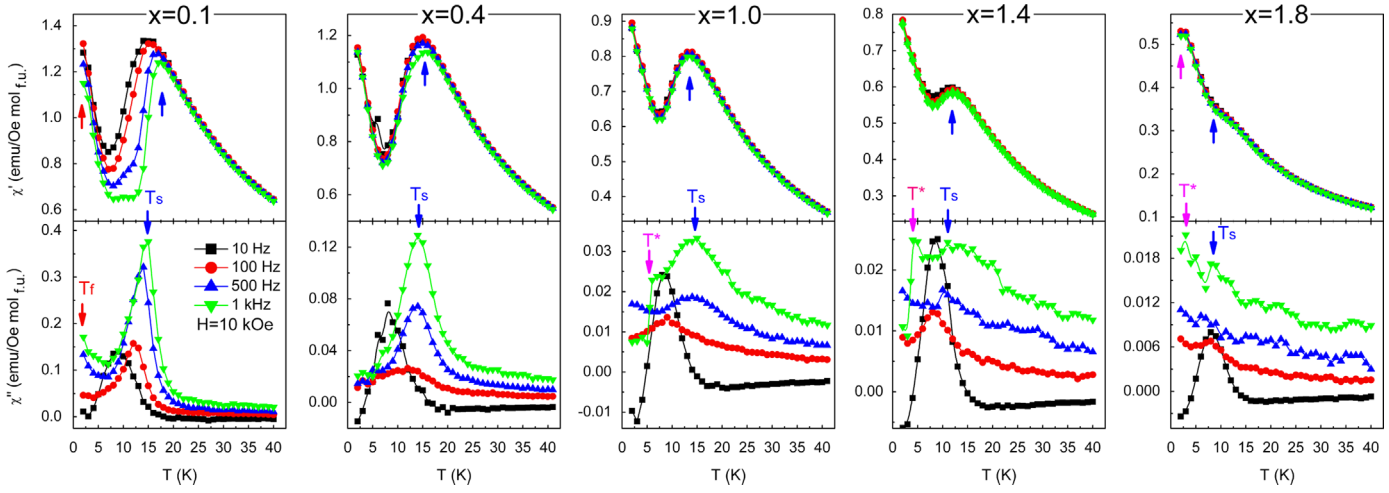

Fig. 7. The real (χ') and imaginary part (χ'') of ac susceptibility of $Dy_{2-x}Yb_xTi_2O_7$ measured at $H=10$ kOe. Marked by the arrows are low-temperature freezing peak (T_f), the single-ion effect peak associated with Dy^{3+} (T_s), and the T^* peak associated with the spin fluctuations of Yb^{3+} (T^*).

interaction is $D=0.018$ K [31]. Therefore, the ferromagnetic interaction in YTO is weaker than that in DTO, hence the FM interaction in doped samples $Dy_{2-x}Yb_xTi_2O_7$ is weaker than that of pure DTO. According to these facts, we suggest that the decrease of long-range dipolar interaction may contribute to the absence of dipolar spin ice.

To investigate the nature of T_s and T^* as well as the spin dynamics in DYTO, we examine the dependence of T_s on frequency by fitting the data to an Arrhenius law

$$f = f_0 \exp(-E_A/k_B T) \tag{3}$$

Where E_A is the activation energy for spin fluctuations and f_0 is a measure of the microscopic limiting frequency in the system [29]. The values of the freezing temperature are obtained from the minimum in the slope of χ''. Unfortunately, T^* appears only at high frequency and the data points are not enough to plot a figure, so only the dependence of T_s on frequency is shown here. As demonstrated in Fig. 8, the frequency dependence of T_s for the $x \leq 0.4$ samples can be well fit to an Arrhenius law, indictive of a thermally activated spin relaxation. The fitted values of E_A and f_0 are also given in Fig. 8. We find that E_A is of the order of the single-ion energy of Dy^{3+} and f_0 is of the order of GHz, which are both reasonable for individual spin flips. The frequency dependence of the T_s peak and the derived energy scale corresponding to the crystal-field splitting are qualitatively similar to that of pure DTO, which verifies that T_s is the single-ion peak of Dy^{3+} spins. When $x \geq 1.0$, the frequency dependence of T_s cannot be fitted to the Arrhenius law, suggesting that the relaxation is not simply thermally activated. The failure of Arrhenius law in the $x \geq 1.0$ samples might be connected to the emergence of a new peak T^* and appearance of a weaker but much more rounded peak T_s. Such a non-Arrhenius behavior has previously been observed in the spin-ice material DTO, where the quantum spin relaxation plays an important role [11]. Therefore, the relaxation process for T_s in high doping samples should be through both thermal activation and quantum tunneling between the two accessible Ising states of Dy^{3+}, which is consistent with the weaker frequency dependence of T_s peaks as well. We suggest that the most likely origin of the quantum tunneling at T_s is the fluctuating dipolar

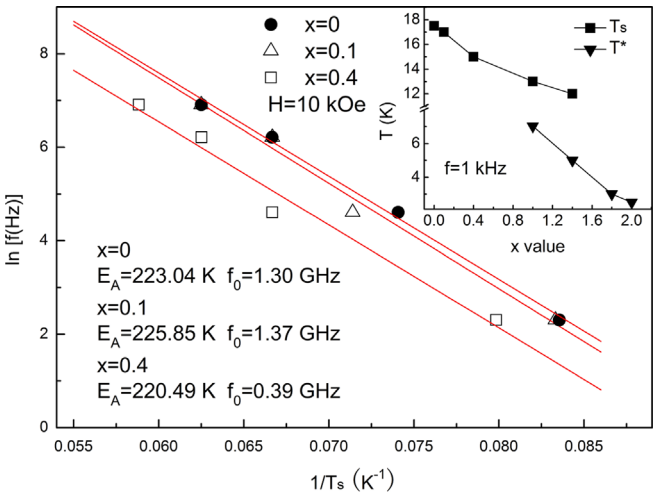

Fig. 8. Arrhenius law fits of the T_s dependence on frequency for the samples of $Dy_{2-x}Yb_xTi_2O_7$ ($x=0$, 0.1, 0.4). The resulting fit parameters f_0 and E_A are also shown. In the inset, the evolution of T_s and T^* with doping content is shown. The values of T_s and T^* are obtained from the maximum in χ' and χ'', respectively.

field arising from the Dy–Yb interactions. In pure DTO, the torque of Dy spins cannot be minimized because of the geometric frustration. However, the introduction of Yb dopants facilitates the spin inversion of Dy^{3+} because the effective field due to Dy–Yb interactions will mix higher states into the ground state doublet. In other words, dopant-assisted processes facilitate the activation of Dy spins.

Since the ground-state Kramers doublet of the CF of Yb^{3+} is separated by 620 K from the first excited state, the thermally activated spin relaxation of single ion should appear at high temperatures. Thus, the peak T^* cannot be assigned as the single-ion peak corresponding to the CF of Yb^{3+}. That is to say, the large barrier is insurmountable at such low temperature as T^*. Mössbauer spectroscopy and muon spin relaxation (μSR) measurements find a rapid decrease of the Yb^{3+} magnetic moments fluctuation rate, upon approaching 0.24 K from above. Above the transition temperature, the fluctuation rate of Yb spins follows a thermal excitation law [18]. Due to this fact, it is suggested that the T^* originates from thermally activated spin fluctuations of Yb, as evidenced by the frequency dependence of the peak T^* in χ'' of YTO. It corresponds to the dynamics of short range correlated spins, perhaps involving spin clusters of Dy and Yb.

It should be noticed that both T_s and T^* move to low temperature with increasing Yb doping content (see the inset of Fig. 8). The doping dependence of T_s should be related to the change of CF levels of Dy^{3+} with the doping of Yb^{3+}. As can be seen from Fig. 1 (b), the lattice parameter of DYTO decreases with increasing Yb doping. One may naively expect that CF splitting of Dy^{3+} and the energy barrier E_A as well as the temperature where the T_s peak locates would increase. However, our result is not consistent with the speculation. Knowing that T_s should be robust against the change in magnetic field [24], we infer that there should be another factor such as CF–phonon coupling contributes in the DYTO system. The doping dependence of T^* should be related to the energy barrier of spin fluctuation of Yb. With the increasing Yb doping, the FM coupling weakens, hence the fluctuations of Yb spins enhance. Consequently, the energy barrier of spin fluctuations decreases and T^* moves to low temperature.

Compared with other mixed frustrated magnets [22–26], the mixing of the rare-earth site in DYTO results in an altered crystal-field scheme as well and the results in DYTO display the similar robustness of both ground states in spite of the complete mixture of the elements. For the present samples, there exist two sets of CF schemes associated with Dy^{3+} and Yb^{3+}, respectively. The peculiar low-temperature behavior is closely associated with the Dy–Yb spin interactions and the altered crystalline electric field. On the analogy of other hybrid pyrochlore compounds, $Dy_{2-x}Yb_xTi_2O_7$ may be considered as mixtures of spin ice (DTO) and quantum spin ice (YTO). It should be also noted that the dilution effect in DYTO is different from that of $Ho_xTb_{2-x}Ti_2O_7$. Since both the Ho^{3+} and Tb^{3+} ions are very Ising like, with a strong preference to lie in the [111] direction, and the dilution only relieve the ice rules slightly [25]. However, Yb^{3+} ions are *XY* like and their easy plane is (111) plane, thus the substitution will relieve the ice rules strongly. Such frustrated materials may offer a medium in investigation of geometrical magnetic frustration.

4. Conclusion

In summary, we have studied the magnetic order and dynamical properties of the spin-frustrated magnet $Dy_{2-x}Yb_xTi_2O_7$. The samples show a tendency towards a relaxed FM interaction on Yb doping, which is related to the decrease of dipolar interactions. With increasing Yb content, a new peak (T^*) associated with Yb^{3+} appears. This peak is originated from thermally activated spin fluctuations of Yb^{3+}. At the same time, the relaxation process for T_s associated with Dy^{3+} is through both thermal activation and quantum tunneling. The low-temperature dynamical behavior is associated with the Dy–Yb spin interactions and the altered crystalline electric field. Moreover, CF-phonon coupling may contribute to the spin dynamic properties.

Acknowledgments

This work was supported by the State Key Project of Fundamental Research of China (Grant nos. 2010CB923403 and 2011CBA00111), the Nature Science Foundation of China (Grant Nos.11174290 and U1232142), and the Hundred Talents Program of the Chinese Academy of Sciences.

References

[1] K. Fritsch, K.A. Ross, Y. Qiu, J.R.D. Copley, T. Guidi, R.I. Bewley, H.A. Dabkowska, B.D. Gaulin, Physical Review B 87 (2013) 094410.
[2] J.S. Gardner, M.J.P. Gingras, J.E. Greedan, Reviews of Modern Physics 82 (2010) 53.
[3] D.J.P. Morris, D.A. Tennant, S.A. Grigera, B. Klemke, C. Castelnovo, R. Moessner, C. Czternasty, M. Meissner, K.C. Rule, J.-U. Hoffmann, K. Kiefer, S. Gerischer, D. Slobinsky, R.S. Perry, Science 326 (2009) 411.
[4] T. Fennell, P.P. Deen, A.R. Wildes, K. Schmalzl, D. Prabhakaran, A.T. Boothroyd, R.J. Aldus, D.F. McMorrow, S.T. Bramwell, Science 326 (2009) 415.
[5] P. Dalmas, de Réotier, A. Yaouanc, Y. Chapuis, S.H. Curnoe, B. Grenier, E. Ressouche, C. Marin, J. Lago, C. Baines, S.R. Giblin, Physical Review B 86 (2012) 104424.
[6] O.A. Petrenko, M.R. Lees, G. Balakrishnan, V.N. Glazkov, S.S. Sosin, Physical Review B 85 (2012) 180412(R).
[7] S.T. Bramwell, M.J.P. Gingras, Science 294 (2001) 1495.
[8] J. Snyder, J.S. Slusky, R.J. Cava, P. Schiffer, Nature (London) 413 (2001) 48.
[9] K. Matsuhira, Y. Hinatsu, T. Sakakibara, Journal of Physics: Condensed Matter 13 (2001) L737.
[10] H. Fukazawa, R.G. Melko, R. Higashinaka, Y. Maeno, M.J.P. Gingras, Physical Review B 65 (2002) 054410.
[11] J. Snyder, B.G. Ueland, J.S. Slusky, H. Karunadasa, R.J. Cava, P. Schiffer, Physical Review B 69 (2004) 064414.
[12] J. Snyder, B.G. Ueland, J.S. Slusky, H. Karunadasa, R.J. Cava, Ari Mizel, P. Schiffer, Physical Review Letters 91 (2003) 107201.
[13] J.A. Hodges, P. Bonville, A. Forget, M. Rams, K. Królas, G. Dhalenne, Journal of Physics: Condensed Matter 13 (2001) 9301.
[14] K.A. Ross, Th. Proffen, H.A. Dabkowska, J.A. Quilliam, L.R. Yaraskavitch, J.B. Kycia, B.D. Gaulin, Physical Review B 86 (2012) 174424.
[15] K.A. Ross, J.P.C. Ruff, C.P. Adams, J.S. Gardner, H.A. Dabkowska, Y. Qiu, J.R. D. Copley, B.D. Gaulin, Physical Review Letters 103 (2009) 227202.
[16] P. Bonville, J.A. Hodges, E. Bertin, J.P. Bouchaud, P. Dalmas, de Réotier, L.-P. Regnault, H.M. Rønnow, J.-P. Sanchez, S. Sosin, A. Yaouanc, Hyperfine interactions 156/157 (2004) 103.

[17] A. Yaouanc, A. Maisuradze, P. Dalmas, de Réotier, Physical Review B 87 (2013) 134405.
[18] J.A. Hodges, P. Bonville, A. Forget, A. Yaouanc, P. Dalmas, de Réotier, G. André, M. Rams, K. Królas, C. Ritter, P.C.M. Gubbens, C.T. Kaiser, P.J.C. King, C. Baines, Physical Review Letters 88 (2002) 077204.
[19] J.S. Gardner, G. Ehlers, N. Rosov, R.W. Erwin, C. Petrovic, Physical Review B 70 (2004) 180404(R).
[20] K.A. Ross, L.R. Yaraskavitch, M. Laver, J.S. Gardner, J.A. Quilliam, S. Meng, J.B. Kycia, D.K. Singh, Th. Proffen, H.A. Dabkowska, B.D. Gaulin, Physical Review B 84 (2011) 174442.
[21] H.B. Cao, A. Gukasov, I. Mirebeau, P. Bonville, Journal of Physics: Condensed Matter 21 (2009) 492202.
[22] L.J. Chang, H. Terashita, W. Schweika, Y.Y. Chen, J.S. Gardner, Journal of Magnetism and Magnetic Materials 310 (2007) 1293.
[23] X. Ke, D.V. West, R.J. Cava, P. Schiffer, Physical Review B 80 (2009) 144426.
[24] H. Xing, M. He, C. Feng, H. Guo, H. Zeng, Z.A. Xu, Physical Review B 81 (2010) 134426.
[25] L.J. Chang, W. Schweika, Y.-J. Kao, Y.Z. Chou, J. Perßon, Th. Brückel, H.C. Yang, Y.Y. Chen, J.S. Gardner, Physical Review B 83 (2011) 144413.
[26] M. Orendáč, P. Vrábel, A. Orendáčová, J. Prokleška, V. Sechovský, S. Singh, R. Suryanarayanan, A. Revcolevschi, Journal of Physics: Condensed Matter 24 (2012) 186003.
[27] D. Prabhakaran, A.T. Boothroyd, Journal of Crystal Growth 318 (2011) 1053.
[28] B.G. Ueland, G.C. Lau, R.J. Cava, J.R. O'Brien, P. Schiffer, Physical Review Letters 96 (2006) 027216.
[29] J. Snyder, B.G. Ueland, Ari Mizel, J.S. Slusky, H. Karunadasa, R.J. Cava, P. Schiffer, Physical Review B 70 (2004) 184431.
[30] X. Ke, R.S. Freitas, B.G. Ueland, G.C. Lau, M.L. Dahlberg, R.J. Cava, R. Moessner, P. Schiffer, Physical Review Letters 99 (2007) 137203.
[31] J.D. Thompson, P.A. McClarty, H.M. Rønnow, L.P. Regnault, A. Sorge, M.J. P. Gingras, Physical Review Letters 106 (2011) 187202.